Study of the Ordered Magnetic State of Copper Formate Tetrahydrate by Antiferromagnetic Resonance*

MOHINDAR S. SEEHRA† AND T. G. CASTNER, JR.
Department of Physics and Astronomy, University of Rochester, Rochester, New York 14627

(Received 25 September 1969)

A brief account of antiferromagnetic-resonance (AFMR) measurements in single crystals of monoclinic $Cu(HCOO)_2\cdot 4H_2O$ has been reported, and it was shown that a model of weak ferromagnetism of the easy-plane type is not consistent with the data. This paper presents in detail the AFMR data and includes calculations of the AFMR modes and the magnetization based on assuming that $Cu(HCOO)_24H_2O$ is very nearly an antiferromagnet in zero magnetic field. AFMR measurements have been made between 1.4 and 15°K. Resonance transitions have been observed at 9 GHz, from 32 to 36 GHz, from 50 to 80 GHz, and from 107 to 124 GHz in magnetic fields up to 26 kOe. From the angular dependence of the field positions of the resonance transitions, a set of "principal axes" $a''bc''$ of the magnetic crystal have been determined. a'', the antiferromagnetic axis, is shown to be 8.5° away from the a axis toward the c axis. The AFMR modes and the magnetization have been calculated on a two-sublattice model, based on a bilinear exchange interaction, assuming a'' as the antiferromagnetic axis, b as the intermediate axis, and c'' as the hard axis. This calculation is an extension of one by Cinader by including the hard-plane anisotropy and an anisotropic antisymmetric g-tensor. It is found that a magnetic field (perpendicular to a'') larger than a critical field induces a weak ferromagnetic state. The calculation also shows that both antisymmetric exchange and the antisymmetric Zeeman interaction contribute to the effective canting fields. For the c''-axis case, the calculations are in good agreement (except for a constant gap in the low-frequency mode above 5.3 kOe) with the data and an effective canting field $H_{DM}'=84$ kOe is obtained. For the b axis, the experiment indicates an instability in the antiferromagnetic axis at 5.3 kOe. The calculations also suggest an instability in the antiferromagnetic axis if a second effective canting field h_{DM}' is negative; however, a quantitative fit to the AFMR modes has not been possible. A simplified calculation for the a'' axis is in fair agreement with some of the a''-axis data. The temperature dependence of the low-frequency zero-field mode is found to deviate substantially from the prediction of the molecular field approximation. A temperature-dependent contribution to the AFMR linewidth of $T^{3.3\pm0.2}$ is found.

I. INTRODUCTION

THE magnetic properties of $Cu(HCOO)_2\cdot 4H_2O$ have attracted considerable attention since Martin and Waterman first suggested[1] that this crystal may behave as a two-dimensional magnetic system as a result of the layer structure[2] and the strong superexchange coupling via the $(HCOO)^-$ ion between the Cu^{2+} ions in the layers. Their magnetic susceptibility measurements on a powder sample above 80°K yielded Θ (Curie-Weiss constant) ≈ 175°K. Subsequent magnetic susceptibility measurements on single crystals, first by Flippen and Friedberg[3] and independently by Kobayashi and Haseda[4] (hereafter referred to as KH), showed a sharp transition at 17°K to the antiferromagnetic state. An additional broad peak in the magnetic susceptibility has been observed near 65°K.[4,5] Using the high-temperature series expansion for the magnetic susceptibility it has been shown[6] that this anomalously large value of Θ/T_N and the broad peak near 65°K can be explained on the basis of two-dimensional Heisenberg antiferromagnetism. A detailed account of the ESR linewidth, including a linear temperature dependence, has been reported.[7] From the temperature-independent exchange-narrowed linewidth the value of the Dzylashinsky-Moriya antisymmetric exchange interaction $\mathfrak{D}\cdot(\mathbf{S}_1\times\mathbf{S}_2)$ (hereafter referred to as the DM interaction) has been obtained.[8]

The magnetization measurements of KH at 4.2°K along L_1, L_2, and L_3, the principal axes of the g tensor, showed[4] that a weak moment appears along L_1 and L_2 with a saturation field of about 5 kOe. This, combined with the sharp peaks at T_N in the magnetic susceptibility along L_1 and L_2, led to the suggestion[3,4] that $Cu(HCOO)_2\cdot 4H_2O$ may be a weak ferromagnet. No neutron diffraction study of the ordered state is available, although KH[3,4] suggested that the spins may be antiparallel along the L_3 axis. From the proton resonance study at 4.2°K, Van Der Leeden *et al.*[9] found that the crystal and magnetic unit cells in $Cu(HCOO)_2\cdot 4H_2O$ are the same.

In order to get information on the nature of the weak ferromagnetism and the spin structure, and to evaluate the exchange parameters which characterize this system,

* Work supported by the U. S. Atomic Energy Commission.

† Present address: Physics Department, West Virginia University, Morgantown, W. Va. 26506.

[1] R. L. Martin and H. Waterman, J. Chem. Soc. 1359 (1959).

[2] R. Kiriyama, H. Ibamoto, and K. Matsuo, Acta Cryst. **7**, 482 (1954).

[3] R. B. Flippen and S. A. Friedberg, J. Chem. Phys. **38**, 2652 (1963); S. A. Friedberg and R. B. Flippen, in *Proceedings of the Seventh International Conference on Low-Temperature Physics, Toronto, 1960*, edited by G. M. Graham and A. C. Hollis Hallett (University of Toronto Press, Toronto, Canada, 1961), p. 122.

[4] H. Kobayashi and T. Haseda, J. Phys. Soc. Japan **18**, 541 (1963); T. Haseda, A. R. Miedema, H. Kobayashi, and E. Kanda, *ibid.* **17B**, 518 (1962).

[5] M. S. Seehra, Rev. Sci. Instr. **39**, 1044 (1968).

[6] M. S. Seehra, Phys. Letters **28A**, 754 (1969).

[7] M. S. Seehra and T. G. Castner, Jr., Physik Kondensierten Materie **7**, 185 (1968).

[8] M. S. Seehra and T. G. Castner, Jr. (unpublished).

[9] P. Van Der Leeden, P. A. Van Dalen, and W. J. M. De Jonge, Physica **23**, 202 (1967).

an antiferromagnetic-resonance (AFMR) study was undertaken. The results of this study are reported in this paper. Based on the experimental results, a model for the spin structure is proposed. The AFMR modes and magnetization curves for the principal directions are calculated and compared with the experiment. A brief description of the experimental data has been reported earlier.[10]

Our preliminary analysis,[10] based on weak ferromagnetism of the easy-plane type, showed that the AFMR data cannot be explained on this model. The question of weak ferromagnetism was unresolved since KH did not measure any hysteresis in the magnetization and the saturation field of 5 kOe is unusually large for a weak ferromagnet. Furthermore, the AFMR measurements showed negligible hysteresis. Recent magnetization measurements by Gyorgy[11] on our crystals showed negligible hysteresis consistent with the AFMR observations. In this paper we show that most of the AFMR and magnetization data can be explained by assuming that $Cu(HCOO)_2\cdot 4H_2O$ is an antiferromagnet (AF) in zero magnetic field. However, by applying a magnetic field **H** perpendicular to the easy axis, the spin system can be brought into a weak ferromagnetic (WF) state.

Such an AF-WF transition was first observed by Borovik-Romanov and Kreines[12] and Kreines[13] in anhydrous $CoSO_4$. A similar transition has since been observed in hematite (α-Fe_2O_3) below the Morin temperature and is the center of considerable attention at present.[14] The AF-WF transition is frequently accompanied by an abrupt increase in the magnetization at a critical magnetic field. In $Cu(HCOO)_2\cdot 4H_2O$, such a discontinuity has been observed along the b axis both in the AFMR[10] modes and in the magnetization[11] at about 5.3 kOe. In $CoSO_4$[13] and hematite[14] the abrupt increase in the magnetization was attributed to the presence of a fourth-order anisotropy parameter. For a spin $S=\frac{1}{2}$ system such as $Cu(HCOO)_2\cdot 4H_2O$, this term contributes only a constant to the free energy. Therefore, the physical mechanism for the discontinuity in $Cu(HCOO)_2\cdot 4H_2O$ is different. We discuss the possibility that the instability could be caused by the antisymmetric Zeeman interaction.

The calculation of the AFMR modes for a Dzylashinsky AF (with $\mathfrak{D}$ along the easy axis) was made by Cinader.[15] Ozhogin and Shapiro[16] extended these calculations for **H** along a general direction. Here, we have extended Cinader's calculations to include the hard-plane anisotropy and also the anisotropic g tensor. The role of antisymmetric g tensors has been considered by other groups. Silvera, Thornley, and Tinkham[17] showed that the antisymmetric g tensor could produce large canting of the sublattices. Turov,[18] while considering the general symmetry requirements for the existence of WF, proved that the antisymmetric g tensor can contribute to WF. Gurevich *et al.*[19] found that the antisymmetric component of the g tensor multiplied by the isotropic exchange in orthorhombic $NaNiF_3$ contributes to the AFMR modes in the same way as the DM interaction. The present case, though similar in some ways, is more complicated because of the lower monoclinic symmetry of $Cu(HCOO)_2\cdot 4H_2O$.

The experimental details are presented in Sec. II, followed by the calculation of the AFMR modes and the magnetization in Sec. III. The experimental results are given in Sec. IV, and comparison with the calculations is made in Sec. V.

II. EXPERIMENTAL

The single crystals of $Cu(HCOO)_2\cdot 4H_2O$ were grown from saturated aqueous solution. The details of the crystal preparation, alignment procedure, etc., have been described elsewhere.[7] Many different crystals were used for the AFMR measurements. Typical dimensions of the crystals used were about $1.5\times 3\times 0.5$ mm.

The AFMR data were taken at 9 GHz, from 33 to 36 GHz, from 50 to 80 GHz, and from 107 to 124 GHz employing four different microwave spectrometers and six klystrons. Owing to insufficient frequency sources, the intervening regions could not be investigated. A Varian 12-in. magnet with auxiliary iron-cobalt pole caps produced a maximum magnetic field of 17.2 and 28.7 kOe in a gap of 1.75 and 0.75 in., respectively. A homemade Dewar with a changeable tail stock was used to fit the various gaps. The spectrometers operating at 3 cm and 8 mm were of conventional design using balanced bolometer detection. The 5- and 2.5-mm spectrometers were comparatively simpler in design,[20] employing straight bolometer detection. Most of the AFMR measurements were made in reflection without a resonance cavity. Instead, a waveguide piece shorted at one end was used. Thus, no frequency stabilization was necessary and the frequency could be varied over

[10] M. S. Seehra and T. G. Castner, Jr., J. Appl. Phys. **40**, 1240 (1969).

[11] E. M. Gyorgy (private communication).

[12] A. S. Borovik-Romanov and N. M. Kreines, Zh. Eksperim. i Teor. Fiz. **35**, 1053 (1958) [English transl.: Soviet Phys.—JETP **8**, 734 (1959)].

[13] N. M. Kreines, Zh. Eksperim. i Teor. Fiz. **40**, 726 (1961) [English transl.: Soviet Phys.—JETP **13**, 534 (1961)].

[14] For a recent work on this transition see P. J. Flanders, J. Appl. Phys. **40**, 1247 (1969). A review of some earlier work on $CoSO_4$ and α-Fe_2O_3 has been given by Jan Kaczer, in *Proceedings of the Tenth International Conference on Low Temperature Physics, Moscow, U.S.S.R., 31 August–6 September 1966* (Viniti Publishing House, Moscow, U.S.S.R., 1967), Vol. IV, p. 6.

[15] G. Cinader, Phys. Rev. **155**, 453 (1967).

[16] V. I. Ozhogin and V. G. Shapiro, Zh. Eksperim. i Teor. Fiz. **54**, 96 (1968) [English transl.: Soviet Phys.—JETP **27**, 54 (1968)].

[17] I. F. Silvera, J. H. M. Thornley, and M. Tinkham, Phys. Rev. **136A**, 695 (1964).

[18] E. A. Turov, in *Physical Properties of Magnetically Ordered Crystals* (Academic Press Inc., New York, 1965), Chap. V.

[19] A. G. Gurevich, V. A. Sanina, E. I. Golovenchits, and S. S. Starobinets, J. Appl. Phys. **40**, 1512 (1969).

[20] M. S. Seehra, Ph.D. thesis, The University of Rochester, 1969 (unpublished).

the entire range of a klystron in a single experiment. The signal-to-noise ratio for the AFMR transitions was sufficient without a cavity. The phase of signal could be adjusted so that either dispersion or absorption could be observed. In all experiments the applied dc field was approximately perpendicular to the oscillating magnetic field. Most of the data were taken at 4.2°K since the temperature dependence below this temperature was found to be negligible. The temperature dependences of some of the transitions were measured between 1.4 and 15°K. A calibrated carbon resistor was used to measure the temperature.

III. THEORETICAL CONSIDERATIONS

A. Spin Configuration

From a study of the magnetic state of $Cu(HCOO)_2 \cdot 4H_2O$ using proton and deuteron magnetic resonance, Van Der Leeden *et al.*[9] concluded that the crystal and magnetic unit cells in this system are the same. Since there are only two inequivalent Cu^{2+} ions per unit cell, the system must be described by a two-sublattice model. Using this fact and the symmetry requirements for a monoclinic crystal as discussed by Turov,[18] we conclude that the antisymmetric exchange vector $\mathfrak{D}$ must be perpendicular to the twofold rotation axis, i.e., it lies in the *ac* plane. In the magnetization measurements of KH[4] there is no evidence of a WF moment at $H=0$. Recent magnetization measurements of Gyorgy[11] have further shown that the hysteresis in the magnetization is negligible. From this and the analysis of the AFMR data we conclude that the system is a good approximation to an AF[21] at $H=0$. From the positions of the extremum resonance fields in the angular dependence of the AFMR (see Figs. 2 and 3) we have determined a set of "principal axes" of the ordered spin system to be the a'', b, and c'' axes.[22] These axes are shown in Fig. 1. (a'' is 8.5° from the crystal a axis towards the c axis.) We will show that much of the AFMR and the magnetization data can be explained if the AF axis is assumed along a'' at $H=0$.

The "principal axes" a'', b, and c'' do not coincide with the principal axes of the g tensor[7] except for b, the twofold rotation axis. Therefore, the g-tensor anisotropy is considered explicitly. The g tensors for the two-ions are written as

$$\begin{vmatrix} g_{11} & \pm g_{12} & \pm g_{13} \\ \pm g_{21} & g_{22} & g_{23} \\ \pm g_{31} & g_{32} & g_{33} \end{vmatrix}, \quad (1)$$

where the + and − signs are, respectively, for the ion No. 1 at (0,0,0) and ion No. 2 at $(\frac{1}{2},\frac{1}{2},0)$. In general, for a monoclinic crystal, $g_{ij} \neq g_{ji}$. However, this asymmetry cannot be determined from a simple ESR experiment.[23] An estimate of various g_{ij}'s in the $a''bc''$ coordinate system has been made from the g-value measurements assuming the g tensor to be symmetric.[20]

B. Free Energy for a Two-Sublattice Model

The phenomenological free energy F based on a two-sublattice model is written as

$$\begin{aligned} F = & J\mathbf{S}_1 \cdot \mathbf{S}_2 \\ & + D(S_{Z1}S_{Z2} - \tfrac{1}{3}\mathbf{S}_1 \cdot \mathbf{S}_2) + E(S_{X1}S_{X2} - S_{Y1}S_{Y2}) \\ & + A(S_{Z1}S_{Y2} + S_{Y1}S_{Z2}) - \mathfrak{D}_Z(S_{X1}S_{Y2} - S_{Y1}S_{X2}) \\ & - \mathfrak{D}_Y(S_{Z1}S_{X2} - S_{X1}S_{Z2}) - \mu_B \mathbf{H} \cdot (\mathbf{g}_1 \cdot \mathbf{S}_1 + \mathbf{g}_2 \cdot \mathbf{S}_2), \end{aligned} \quad (2)$$

where X is taken along b (the twofold symmetry axis), Y along c'', and Z along a''. J represents the isotropic exchange, D and E are diagonal components of the symmetric anisotropic exchange, A is the off-diagonal component of symmetric anisotropic exchange allowed by symmetry,[24] $\mathfrak{D}_Z$ and $\mathfrak{D}_Y$ are the components of the DM interaction allowed by symmetry; the last term is just the Zeeman interaction. D, E, and $\mathfrak{D}_Z$ are defined positive so that for the case considered here ($S=\frac{1}{2}$) if we neglect the effects of the A term, Z will be the easy axis, X is the intermediate axis, and Y is the hard axis for $D>E$. Equation (2) contains the most general bilinear intersublattice exchange interaction allowed by monoclinic symmetry for the $S=\frac{1}{2}$ case. It is noted that for $S=\frac{1}{2}$ systems, the single-ion anisotropy terms $D_1S_{Z1}^2$, etc., and the higher-order biquadratic exchange interaction terms of the form $S_{Z1}^2S_{Z2}^2$, etc., are constants and need not be included in Eq. (2). Intrasublattice anisotropic exchange can also contribute to the frequency of AFMR modes.[17,25] However, in the present case intrasublattice exchange is thought to be negligible.[6] The calculations below follow the general procedures of those by Herrmann.[26] Insofar as possidle we have followed the notation of Cinader.[15]

C. $\mathbf{H} \| Y$ Axis (c'' Axis)

1. *Equilibrium Conditions*

For the case $H \| Y$ we employ the angles θ, ϕ, and α as shown in Fig. 1(a). θ measures the cant of the AF axis from the Z axis in the ZX plane, while ϕ measures the cant of the two sublattices toward the magnetic

[21] Because of one of the antisymmetric components of the g tensors, there can be a net magnetization of the two sublattices even when they are exactly antiparallel (AF). A small cant of the two sublattices is possible and can be very hard to determine.

[22] These are "principal axes" as inferred from the angular dependence of the AFMR modes. As is shown by the mode calculations, it is not readily transparent that these axes are the principal axes of the exchange interaction.

[23] F. K. Kneubuhl, Phys. Letters **2**, 163 (1962); F. S. Ham, J. Phys. Chem. Solids **24**, 1165 (1963); F. K. Kneubuhl, Physik Kondensierten Materie **1**, 410 (1963).

[24] The calculations which follow were first done with A and $\mathfrak{D}_Y$ equal to zero. As will be shown, the effect of these terms on the $\mathbf{H} \| Y$-axis case is very minor, while the effect on the $H \| X$-axis case is to alter some of the parameters but not to alter the form of the equilibrium conditions, the magnetization, or the AFMR modes. Without accurate knowledge of the off-diagonal g-tensor components and some of the exchange parameters it is very difficult to assess whether A and $\mathfrak{D}_Y$ make a significant contribution to the magnetic behavior.

[25] M. Date, J. Phys. Soc. Japan **16**, 1337 (1961).

[26] G. F. Herrmann, J. Phys. Chem. Solids **24**, 597 (1963).

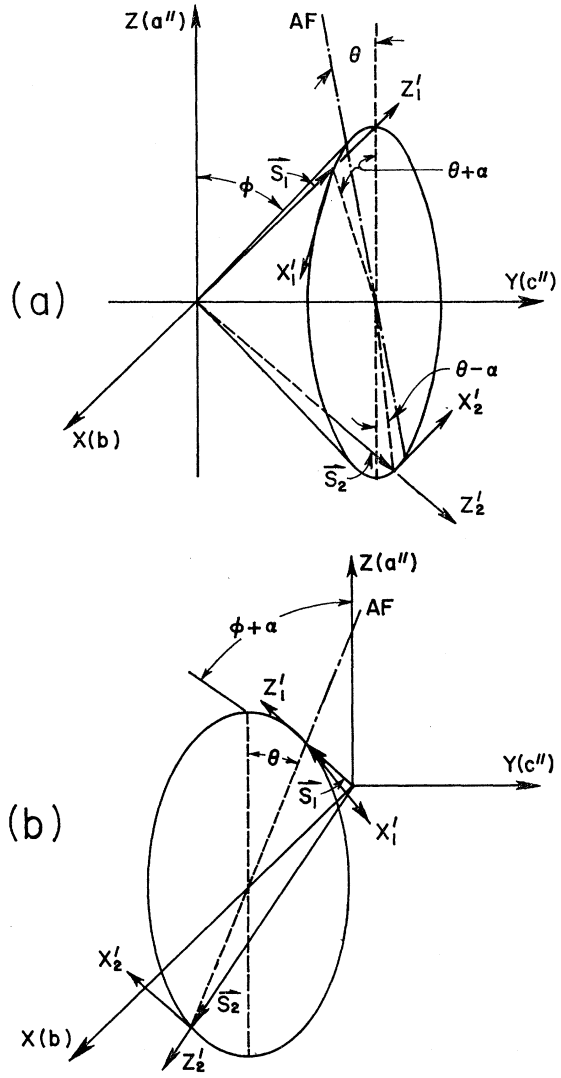

FIG. 1. Equilibrium coordinates: the primed coordinates used for calculating the AFMR modes. At zero field Z is the AF axis ($\mathbf{S}_1-\mathbf{S}_2$). (a) is for the magnetic field along the Y axis; (b) is for the magnetic field along the X axis. X_i', Y_i', Z_i' $(i=1,2)$ are components of a unit vector. X_i' is tangent to the base boundary of the cone so that when $\theta=0$ $X_i'\|(-1)^{i+1}X$ if $\alpha=0$ for case (a), while $X_i'\|(-1)^{i+1}Y$ for case (b). Y_i' is defined so as to make X_i', Y_i', Z_i' a right-handed system. θ is the angle between the AF axis and the Z axis. ϕ is the canting angle of the spins (of the cone) out of the ZX plane in (a), while $\phi'=\phi+\alpha$ is the canting angle out of the ZY plane for (b). α is a possible initial cant in zero field of the two sublattices away from Z in the ZX plane.

field (Y axis). α represents a constant initial cant of the two sublattices in the ZX plane caused by the $\mathfrak{D}_y$ component of the DM interaction. Using Eq. (1) and these angles, we can write Eq. (2) as

$$\begin{aligned}\mathfrak{IC}=&H_{ex}(\sin^2\alpha-\cos^2\alpha\cos2\phi)-H_K\cos^2\phi(\cos^2\theta-\sin^2\alpha)\\&+H_{K'}[\cos^2\phi(\sin^2\alpha-\sin^2\theta)-\sin^2\phi]\\&-H_A\sin\alpha\sin2\phi\sin\theta-H_{DM}\cos\alpha\sin2\phi\sin\theta\\&-h_{DM}\sin2\alpha\cos^2\phi-H(g_{21}'\cos\alpha\cos\phi\sin\theta\\&+g_{22}\sin\phi-g_{23}'\sin\alpha\cos\phi\sin\theta),\end{aligned}\tag{3}$$

where

$$\begin{aligned}&\mathfrak{IC}\equiv F\langle S\rangle/2\mu_B,\quad H_{ex}=(J-\tfrac{1}{3}D)\langle S\rangle/2\mu_B,\\&H_K=D\langle S\rangle/2\mu_B,\quad H_{K'}=E\langle S\rangle/2\mu_B,\quad H_A=A\langle S\rangle/2\mu_B,\\&H_{DM}=\mathfrak{D}_Z\langle S\rangle/2\mu_B,\quad h_{DM}=\mathfrak{D}_Y\langle S\rangle/2\mu_B,\end{aligned}$$

and

$$H_{K^{\pm}}=H_K\pm H_{K'}.\tag{4}$$

The equilibrium conditions are obtained for a fixed magnetic field by setting $\partial\mathfrak{IC}/\partial\theta=0$ and $\partial\mathfrak{IC}/\partial\phi=0$. After solving these two conditions for $\sin\theta$ and $\sin\phi$, respectively, one finds

$$\sin\theta\approx H_Y H_{DM'}/H_{11c}^2,\qquad H<H_0\tag{5a}$$

$$\sin\phi\approx H_Y[H_{K^-}+(g_{21}'/g_{22})H_{DM}]/H_{11c}^2,\quad H<H_0\tag{5b}$$

and

$$\sin\theta=1,\qquad H>H_0\tag{6a}$$

$$\sin\phi\approx[H_{DM}+H_Y]/2H_{ex},\qquad H>H_0\tag{6b}$$

where

$$\begin{aligned}&H_{DM'}\simeq H_{DM}+2H_{ex}(g_{21}'/g_{22}),\\&H_{11c}^2\simeq(2H_{ex}+H_{K^-})H_{K^-}-H_{DM}^2,\\&g_{21}'=g_{21}\cos\alpha-g_{23}\sin\alpha,\\&H_0=H_{11c}^2/(\tfrac{1}{2}g_{22}H_{DM'}).\end{aligned}\tag{7}$$

In these expressions $H_Y=(\frac{1}{2}g_{22})H$ is a "modified" magnetic field along the Y axis; $H_{DM'}$ represents the effective canting field for this geometry due to both the DM interaction and the antisymmetric Zeeman interaction; while H_{11c} corresponds to the spin-flop field of a simple antiferromagnet (no canting of the AF axis). H_{11c} will be the same as in Cinader's case[15] if one sets $H_{K'}=0$ and $\alpha=0$ (i.e., $h_{DM}=0$). The critical field H_0 corresponds to a 90° rotation of the AF axis $\mathbf{S}_1-\mathbf{S}_2$ from along the Z axis to along the X axis.

2. *Magnetization*

Using Eq. (1) and the geometry of Fig. 1(a), we can write the component of the magnetization along Y, M_Y, as

$$M_Y=N\mu_B\langle S\rangle(g_{21}'\cos\phi\sin\theta+g_{22}\sin\phi).\tag{8}$$

Employing Eqs. (5a), (5b), (6a), and (6b) one obtains

$$\begin{aligned}M_Y=&(Ng_{22}\mu_B\langle S\rangle H_Y/2H_{ex})\\&\times[1+(H_{DM'}/H_{11c})^2],\quad H<H_0\end{aligned}\tag{9a}$$

and

$$M_Y=(Ng_{22}\mu_B\langle S\rangle/2H_{ex})[H_{DM'}+H_Y],\quad H>H_0.\tag{9b}$$

According to Eq. (9b) the system is in the WF state for $H>H_0$, and the first term in Eq. (9b) gives the magnitude of the WF moment. From Eqs. (9a) and (9b), the ratio of the magnetic susceptibility $\chi_{\perp,Y}^{AF}$ in the AF state (for $H<H_0$) to $\chi_{\perp,Y}^{WF}$, the susceptibility in the WF state, is given by

$$\chi_{\perp,Y}^{AF}/\chi_{\perp,Y}^{WF}=1+(H_{DM'}/H_{11c})^2.\tag{10}$$

Equation (10) shows that $\chi_{1,Y}^{AF} > \chi_{1,Y}^{WF}$. Comparison of Eq. (10) with the experimental data is made in Sec. V.

3. AFMR Modes

To obtain the AFMR frequencies, we employ the usual small-signal approximation used by Herrmann[26] and Cinader.[15] This is done by expressing the motion of the spin vectors in terms of their spin deviations from equilibrium. The Hamiltonian is transformed into new equilibrium coordinate systems X_i', Y_i', Z_i' ($i=1,2$) as shown in Fig. 1(a). Let the component of the unit vector $\mathbf{R}_i=\mathbf{S}_i/\langle S\rangle$ be denoted by X_i', Y_i', Z_i'. Here Z_i' is the equilibrium position of the spin $\mathbf{S}_i$. The transformation equations are similar to those of Cinader,[15] but differ because $\alpha\neq 0$. They are ($i=1,2$)

$$\begin{aligned} X_i &= (-1)^{i+1}\cos(\theta+\alpha_i)X_i' \\ &\quad +(-1)^i \sin\phi \sin(\theta+\alpha_i)Y_i' \\ &\quad +(-1)^{i+1}\cos\phi \sin(\theta+\alpha_i)Z_i', \\ Y_i &= \cos\phi\, Y_i' + \sin\phi\, Z_i', \\ Z_i &= (-1)^i \sin(\theta+\alpha_i)X_i' \\ &\quad +(-1)^i \sin\phi \cos(\theta+\alpha_i)Y_i' \\ &\quad +(-1)^{i+1}\cos\phi \cos(\theta+\alpha_i)Z_i', \end{aligned} \tag{11}$$

where $\alpha_1=+\alpha$ and $\alpha_2=-\alpha$. Substituting (11) into (2), one obtains the following Hamiltonian:

$$\begin{aligned} \mathcal{H} &= AX_1'X_2'+BY_1'Y_2'+CZ_1'Z_2'+K(Y_1'Z_2'+Z_1'Y_2') \\ &\quad +F(X_1'Y_2'+Y_1'X_2')+G(Z_1'X_2'+X_1'Z_2') \\ &\quad +a(X_1'+X_2')+b(Y_1'+Y_2')+c(Z_1'+Z_2'), \end{aligned} \tag{12}$$

where the constants in Eq. (12) are functions of θ, ϕ, and α and will be given below for specific field directions. Employing the relations $(i/\gamma)(d\mathbf{R}_i/dt)=[\mathbf{R}_i,\mathcal{H}]$, where γ is the gyromagnetic ratio (and enters here through our definition of $\mathcal{H}$), taking the time dependence of X_i' and Y_i' in the form $e^{i\omega t}$ and solving the resulting set of linearized equations we obtain the following expression for the AFMR modes:

$$(\omega_\pm/\gamma)^2=(C+c\pm A)(C+c\pm B)-F^2. \tag{13}$$

For the specific case $\mathbf{H}\|Y$ the necessary constants are

$$\begin{aligned} A_Y &= -H_{ex}\cos 2\alpha - H_{K^-}\sin^2\theta + H_{K^+}\sin^2\alpha \\ &\quad -H_{K'}-h_{DM}\sin 2\alpha, \\ B_Y &= H_{ex}[1-(1+\cos 2\alpha)\sin^2\phi] \\ &\quad -H_{K^-}\sin^2\phi\cos^2\theta+H_{K^+}\sin^2\phi\sin^2\alpha \\ &\quad -H_{K'}-h_{DM}\sin 2\alpha\sin^2\phi \\ &\quad +(H_{DM}\cos\alpha+H_A\sin\alpha)\sin 2\phi\sin\theta, \\ C_Y &= H_{ex}[-\cos 2\alpha+(1+\cos 2\alpha)\sin^2\phi] \\ &\quad -H_{K^-}\cos^2\phi\cos^2\theta+H_{K^+}\cos^2\phi\sin^2\alpha \\ &\quad -H_{K'}-h_{DM}\sin 2\alpha\cos^2\phi \\ &\quad -(H_{DM}\cos\alpha+H_A\sin\alpha)\sin 2\phi\sin\theta, \\ F_Y &= -H_{K^-}\sin\phi\sin\theta\cos\theta \\ &\quad -(H_{DM}\cos\alpha+H_A\sin\alpha)\sin 2\phi\sin\theta, \\ c_Y &= -\tfrac{1}{2}H[g_{21}'\cos\phi\sin\theta+g_{22}\sin\phi]. \end{aligned} \tag{14}$$

Equations (13) and (14) have been presented in a slightly different form from that of Cinader's expressions; nevertheless, the expressions are identical to his when one sets $H_{K'}=0$, $h_{DM}=0$, and makes the g tensors isotropic and diagonal. Employing Eqs. (5), (6), (13), and (14), we can find the AFMR modes for the following special cases:

case I: $H<H_0$,

$$(\omega_+/\gamma)^2\approx H_{11b}^2+H_Y^2, \tag{15a}$$

$$(\omega_-/\gamma)^2=H_{11c}^2-H_Y^2(H_{DM}'/H_{11c})^2, \tag{15b}$$

where

$$H_{11b}^2\approx(2H_{ex}+H_{K^+})H_{K^+}+h_{DM}^2-H_{DM}^2;$$

case II: $H>H_0$,

$$(\omega_+/\gamma)^2\approx H_{11b}^2+H_Y^2+\tfrac{1}{2}g_{22}(H-H_0)H_{DM}', \tag{16a}$$

$$(\omega_-/\gamma)^2\approx H_Y H_{DM}'-H_{11c}^2=\tfrac{1}{2}g_{22}(H-H_0)H_{DM}'. \tag{16b}$$

These expressions are identical to those found by Cinader if one requires $H_{11b}=H_{11c}$. We note that the zero-field splitting of the two modes is due to both the hard-plane anisotropy constant, $H_{K'}$, and the Y component of the DM interaction, h_{DM} [$\mathfrak{D}_Y$ in Eq. (2)].

D. $\mathbf{H}\|X$ Axis (b Axis)

For this case the cone shown in Fig. 1(a) is rotated 90° so that its axis is along X as shown in Fig. 1(b). Owing to the Y component of the DM interaction there is a constant cant in zero magnetic field of α of each sublattice from the Z axis (in the ZX plane). The angle $\phi'=\phi+\alpha$ is the total cant angle of the cone, ϕ being the cant induced by the magnetic field. The tilt of the AF axis from the Z direction is designated by θ and corresponds to a rotation of the AF axis in the ZY plane [note that θ in Fig. 1(b) has the opposite sense of that in Fig. 1(a)]. The free-energy Hamiltonian for this case is readily shown to be

$$\begin{aligned} \mathcal{H} &= -H_{ex}\cos 2\phi' - H_{K^+}\cos^2\phi' + H_{K'} - H_A\cos^2\phi'\sin 2\theta \\ &\quad +(H_{DM}\sin\theta-h_{DM}\cos\theta)\sin 2\phi' \\ &\quad -H(g_{11}\sin\phi'+g_{12}\cos\phi'\sin\theta+g_{13}\cos\phi'\cos\theta). \end{aligned} \tag{17}$$

1. Equilibrium Conditions

Minimizing $\mathcal{H}$ with respect to θ, one obtains from Eq. (17)

$$\begin{aligned} &H_{K^+}\cos\phi'\sin\theta+(\tfrac{1}{2}g_{13}H+h_{DM}\sin\phi')\tan\theta \\ &\quad =\tfrac{1}{2}g_{12}H-H_{DM}\sin\phi'+H_A\cos\phi'(\cos 2\theta/\cos\theta). \end{aligned} \tag{18}$$

As H approaches zero, ϕ and θ must also go to zero. Equation (18) indicates that for this to be true H_A must be given by

$$H_A=H_{DM}\tan\alpha. \tag{19}$$

Note that if Eq. (19) is not satisfied in zero field then θ cannot be zero and $Z(c'')$ will not be the AF axis. Differentiating Eq. (17) with respect to ϕ yields a more complex equilibrium condition which is accurately

approximated by

$$\sin\phi' \approx [\tfrac{1}{2}g_{11}H + h_{\mathrm{DM}}\cos\theta - H_{\mathrm{DM}}\sin\theta]/2H_{\mathrm{ex}}, \quad (20)$$

where $\sin\phi' \ll 1$ and $\cos\phi' \sim 1$. Again the requirement that ϕ and θ approach zero as H goes to zero yields a condition on h_{DM}, namely,

$$h_{\mathrm{DM}} = (2H_{\mathrm{ex}} + H_{K^+})\tan 2\alpha. \quad (21)$$

Substitution of (20) into (18) yields the equilibrium condition for θ analogous to (5a) (for the Y-axis case). It is

$$\sin\theta + H_X h_{\mathrm{DM}'}\tan\theta/H_{11b}^2 \approx H_X H_{\mathrm{DM}''}/H_{11b}^2, \quad (22)$$

where

$$\begin{aligned} H_{\mathrm{DM}''} &= -H_{\mathrm{DM}} + 2H_{\mathrm{ex}}(g_{12}/g_{11}), \\ h_{\mathrm{DM}'} &= h_{\mathrm{DM}} + 2H_{\mathrm{ex}}(g_{13}/g_{11}), \end{aligned} \quad (23)$$

and $H_X = (g_{11}/2)H$ is the "modified" magnetic field for the X axis. Equation (22) differs in a very fundamental way from (5a) because of the extra term with the $\tan\theta$ dependence. If $h_{\mathrm{DM}'} > 0$ this term will keep θ from reaching $\frac{1}{2}\pi$ (for the c''-axis case $\theta = \frac{1}{2}\pi$ for $H > H_0$) regardless of the size of the magnetic field. If $h_{\mathrm{DM}'} < 0$ this term will cause $\sin\theta$ to increase more rapidly than linearly with the field and can actually produce an instability of the AF axis at a critical angle. This is readily demonstrated by calculating $\partial^2\mathcal{H}/\partial^2\theta$ from (17) [$\partial^2\mathcal{H}/\partial\theta^2 > 0$ for stability of the AF axis]. $\partial^2\mathcal{H}/\partial\theta^2$ can be found as a function of only θ using Eq. (18), conditions (19) and (21), and Eq. (20). The result is

$$\frac{\partial^2\mathcal{H}}{\partial\theta^2} = \frac{1}{H_{\mathrm{ex}}}\left(2H_{\mathrm{ex}}H_{K^+}\cos^2\phi'\cos^2\theta + h_{\mathrm{DM}}^2\cos 2\phi' + \frac{H_X h_{\mathrm{DM}'}\cos\phi'}{\cos\theta}\right). \quad (24)$$

Equation (23) indicates that for $h_{\mathrm{DM}'}$ negative $\partial^2\mathcal{H}/\partial\theta^2$ will approach zero for $\theta < \frac{1}{2}\pi$. If this happens at a critical magnetic field H_c where $\partial^2\mathcal{H}/\partial\theta^2 \sim 0$, one can calculate from Eq. (24) the critical angle θ_c if the parameters are known. For $H > H_c$, the AF-axis angle θ has presumably jumped to a new stable position satisfying the equilibrium condition [Eq. (22)]. However, the lack of significant hysteresis in the magnetization curve for $\mathbf{H} \| X$ (b axis) suggests that the new equilibrium position must also have $\partial^2\mathcal{H}/\partial\theta^2 \sim 0$ for H just above H_c. This requirement rules out $\frac{1}{2}\pi < \theta < \frac{3}{2}\pi$ and suggests that θ jumps to the fourth quadrant, perhaps to approximately $-\theta_c$. [It cannot jump exactly to $-\theta_c$, since this is inconsistent with the equilibrium condition in Eq. (22).] Using Eq. (22) one finds the critical angles $\theta_{c1}(H \to H_c^-)$ and $\theta_{c2}(H \to H_c^+)$ to be given, noting that $h_{\mathrm{DM}'}$ must be negative, by

$$[1 - \lambda/\cos\theta_{c1}]\sin\theta_{c1} = \lambda H_{\mathrm{DM}''}/|h_{\mathrm{DM}'}|, \quad (25a)$$

$$[1 - \lambda/\cos\theta_{c2}]\sin\theta_{c2} = \lambda H_{\mathrm{DM}''}/|h_{\mathrm{DM}'}|, \quad (25b)$$

where $\lambda = (\frac{1}{2}g_{11}H_c)|h_{\mathrm{DM}'}|/H_{11b}^2$ is a positive constant less than 1. Since θ_{c2} has the opposite sign of the θ_{c1}, the square bracket in (25a) must be positive ($\lambda/\cos\theta_{c1} < 1$) while in (25b) it must be negative ($\lambda/\cos\theta_{c2} > 1$). This requires that $|\sin\theta_{c2}| > |\sin\theta_{c1}|$. The stability condition [Eq. (24)] implies that the ratio $\cos\theta_{c2}/\cos\theta_{c1}$ should be close to 1 to maintain reversibility (minimum hysteresis) for increasing and decreasing fields. It is difficult to determine these critical angles from (25a) and (25b) since $H_{\mathrm{DM}''}$ and $h_{\mathrm{DM}'}$ are not known. However, the AFMR modes for $\mathbf{H} \| X$ (b axis) indicate that there is an instability and imply $h_{\mathrm{DM}'} < 0$. It will be shown later how θ_{c2} and θ_{c1} may be determined, in principle, from the AFMR modes.

2. Magnetization

The magnetization component M_X for $M \| b$ is readily shown to be

$$M_X = N\mu_B\langle S\rangle \times (g_{11}\sin\phi' + g_{12}\cos\phi'\sin\theta + g_{13}\cos\phi'\cos\theta). \quad (26)$$

Employing (20) and setting $\cos\phi' \sim 1$, M_X becomes

$$M_X = \frac{N\mu_B\langle S\rangle g_{11}}{2H_{\mathrm{ex}}}(H_X + H_{\mathrm{DM}''}\sin\theta + h_{\mathrm{DM}'}\cos\theta). \quad (27)$$

This expression predicts a nonzero magnetization at zero field ($\theta = 0$) which is in contradiction with the results of KH.[4] The change in the magnetization, $M_X(H) - M_X(0)$, can be calculated for $H < H_c$ using (22) and $1 - \cos\theta = 2\sin^2(\frac{1}{2}\theta) \approx \frac{1}{2}\sin^2\theta$. The result is

$$M_X(H) - M_X(0) = \frac{N\mu_B\langle S\rangle g_{11}^2 H}{4H_{\mathrm{ex}}} \times \left[1 + \left(\frac{H_{\mathrm{DM}''}}{H_{11b}}\right)^2 \frac{1}{[1 - (\lambda/\cos\theta)(H/H_c)]} - \frac{g_{11}h_{\mathrm{DM}'}}{4}\frac{H_{\mathrm{DM}''}^2 H^2}{H_{11b}^2[1 - (\lambda/\cos\theta)(H/H_c)]^2}\right]. \quad (28)$$

The low-field ($H \ll H_c$) AF magnetic susceptibility $\chi_{\perp,X}^{\mathrm{AF}}$ is given by

$$\chi_{\perp,X}^{\mathrm{AF}} \approx \frac{N\mu_B\langle S\rangle g_{11}^2}{4H_{\mathrm{ex}}}\left[1 + \left(\frac{H_{\mathrm{DM}''}}{H_{11b}}\right)^2\right], \quad H \ll H_c. \quad (29)$$

It is difficult to obtain an analytical expression for the magnetization for $H \sim H_c$ and $H > H_c$ because of the more complex equilibrium condition. These expressions will be compared with the experimental results in Sec. V.

3. AFMR Modes

The same general procedure used for the $H \| Y$ axis (c'' axis) case is used for this case; however, the geometry is that of Fig. 1(b). For this case the trans-

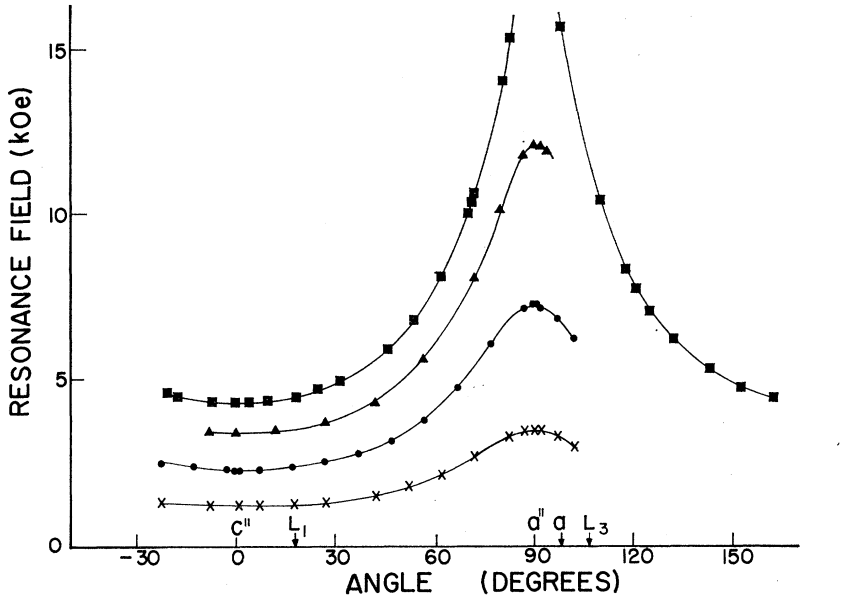

FIG. 2. Angular dependence of the resonance field for the low-field branch of ω_- in the ac plane at 4.2°K. The solid lines are smooth curves through the data points. ■: 36.3 GHz; ▲: 50.4 GHz; ●: 59.6 GHz; X: 64.9 GHz.

formation equations have the form

$$X_i = -\cos\phi'\, Y_i' + \sin\phi'\, Z_i',$$
$$Y_i = (-1)^{i+1}\cos\theta\, X_i' + (-1)^{i+1}\sin\theta\sin\phi'\, Y_i' + (-1)^{i+1}\sin\theta\cos\phi'\, Z_i', \quad (30)$$
$$Z_i = (-1)^{i}\sin\theta\, X_i' + (-1)^{i+1}\cos\theta\sin\phi'\, Y_i' + (-1)^{i+1}\cos\theta\cos\phi'\, Z_i'.$$

Substituting (30) into (2) one finds the necessary coefficients of the transformed Hamiltonian [see Eq. (12)] to be

$$A_X = -H_{ex} - H_{K^+}\sin^2\theta + H_{K'} + 2H_A\sin\theta\cos\theta,$$
$$B_X = H_{ex}\cos 2\phi' - H_{K^+}\cos^2\theta\sin^2\phi' + H_{K'} - 2H_A\sin\theta\cos\theta\sin^2\phi' + (h_{DM}\cos\theta - H_{DM}\sin\theta)\sin 2\phi',$$
$$C_X = -H_{ex}\cos 2\phi' - H_{K^+}\cos^2\theta\cos^2\phi' + H_{K'} - 2H_A\sin\theta\cos\theta\cos^2\phi' - (h_{DM}\cos\theta - H_{DM}\sin\theta)\sin 2\phi', \quad (31)$$
$$F_X = H_{K^+}\sin\theta\cos\theta\sin\phi' - 2H_A\cos 2\theta\sin\phi' - (H_{DM}\cos\theta + h_{DM}\sin\theta)\cos\phi',$$
$$c_X = -\tfrac{1}{2}H(g_{11}\sin\phi' + \sin\theta\cos\phi'\, g_{12} + \cos\theta\cos\phi'\, g_{13}).$$

Using (13) and eliminating $\sin\phi'$ with Eq. (20) the AFMR modes for $H\|X$, neglecting higher-order contributions, are

$$(\omega_+/\gamma)^2 = H_{\|c}^2 - H_{\|b}^2\sin^2\theta + H_X H_{DM}^* + H_X^2, \quad (32a)$$
$$(\omega_-/\gamma)^2 = H_{\|b}^2(1-2\sin^2\theta) + H_X H_{DM}^*, \quad (32b)$$

where

$$H_{DM}^* = H_{DM''}\sin\theta + h_{DM'}\cos\theta. \quad (33)$$

H_{DM}^* is an effective canting field, which unlike the Y-axis (c''-axis) case, contains two components with different field dependences. Although (32a) and (32b) still contain θ as a field-dependent parameter, the field dependence of the modes can be found if the equilibrium condition Eq. (22) can be solved. It will be shown in Sec. V that these equations give a satisfactory qualitative explanation of the unusual AFMR mode behavior found for $H\|X$ axis.

E. H$\|Z$ (a'' Axis)

This case is much more difficult to analyze than the preceding cases. In general, the magnetic field **H** is no longer symmetrical with respect to $\mathbf{S}_1$ and $\mathbf{S}_2$ in equilibrium. It is no longer possible to describe the equilibrium condition with just two angles θ and ϕ. Furthermore, the magnetic field now couples the normal-mode eigenvectors of the two previous cases (namely, $X_1'+X_2'$, $Y_1'+Y_2'$ and $X_1'-X_2'$, $Y_1'-Y_2'$), so that the determinant no longer reduces to two 2×2 determinants. However, an approximate solution is readily obtainable if the effect of the canting field (i.e., $H_{DM'}$, $H_{DM''}$, and $h_{DM'}$) are neglected in determining the equilibrium position—namely, the equilibrium positions of the two sublattices are assumed to remain antiparallel (AF) along the Z axis for the magnetic field below the critical field determined by the spin-flop condition. The calculation becomes similar to the uniaxial case discussed by Foner and Williamson[27] for α-Fe_2O_3 below its Morin temperature. However, it differs because of the additional hard-plane anisotropy field $H_{K'}$ which removes the degeneracy of the two modes at zero field. As shown in the Appendix the frequencies of the two modes for **H** $\|$ a'' are given by

$$(\omega_\pm/\gamma)^2 = \tfrac{1}{2}(H_{\|b}^2 + H_{\|c}^2) + H_Z^2 \pm [\tfrac{1}{4}(H_{\|b}^2 - H_{\|c}^2)^2 + 2(H_{\|b}^2 + H_{\|c}^2)H_Z^2]^{1/2}, \quad (34)$$

where $H_Z = (\frac{1}{2}g_{33})H$ is the "modified" magnetic field

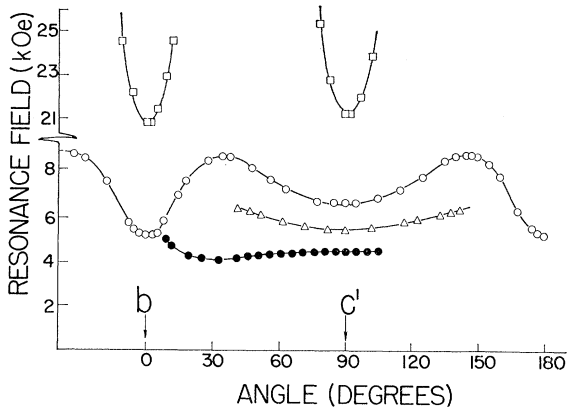

FIG. 3. Angular dependence of the resonance field for the ω_- mode in the bc' plane at 4.2°K. □: 120.0 GHz; ○: 59.8 GHz; △: 50.3 GHz; and ●: 36.3 GHz. The solid lines are smooth curves through the data points.

along the Z axis. $H_{\|b}$ and $H_{\|c}$ are just the zero-field frequencies of the two modes. It should also be noted that the temperature-dependent correction due to a finite $\chi_\|/\chi_\perp$ has been neglected ($\chi_\|$ assumed zero).

Setting $H_{\|b}=H_{\|c}$, one observes that (34) reduces to $(\omega_\pm/\gamma)=H_{\|c}\pm H_Z$ which is exactly the same as the Foner-Williamson expression.[27] However, for $H_{\|b}\gg H_{\|c}$, the lower mode ω_- is approximated by $(\omega_-/\gamma)^2=H_{\|c}^2-H_X^2$. Both these expressions lead to a critical field for spin-flop of $H_{c\,\text{spin-flop}}=(2/g_{33})H_{\|c}$. For $H_{\|b}$, somewhat larger than $H_{\|c}$, the mode curve will lie between the linear expression of Foner and Williamson and the curve $(\omega_-/\gamma)=(H_{\|c}^2-H_X^2)^{1/2}$.

IV. EXPERIMENTAL RESULTS

In Fig. 2 we have shown the angular dependence of the resonance field for the low-field branch of the low-frequency mode ω_- at four different frequencies.[28] The positions of the minimum and the maximum resonance fields are, respectively, c'' and a'' axis. The resonance line is broader along a'' than along c''. The angular dependence of the high-field branch of the ω_- mode is quite similar to the data at 36.3 GHz in Fig. 2, viz., the resonance along a'' could not be observed with the available magnetic field and the minimum is also along c''.

The angular dependence of ω_- in the bc' [29] plane is shown in Fig. 3. The frequency dependence of the angular dependence will become clear when we discuss the AFMR modes along the b axis. The relevant fact in the present context is that the resonance field is an extremum along the b and c' directions. The additional extrema at positions in between the b and c' axes are not 90° apart and their position is magnetic-field-dependent. This suggests that these positions do not correspond to the principal axes. From the above angular dependence we conclude, as noted earlier in Sec. III, that a'', b, and c'' are the "principal axes" for the ordered spin system. Therefore, most of the data were taken along these directions.

A. AFMR Modes for H‖c″

The AFMR frequency–versus–magnetic-field diagram for $\mathbf{H}\|c''$ is shown in Fig. 4. The zero-field frequency for ω_- is 67.3 GHz at 4.2°K. The resonance frequency decreases as the magnetic field is increased extrapolating to zero at $H_0=5.25$ kOe. Above H_0, a high-frequency mode ω_+ and a low-frequency mode ω_- are observed. The low-field branch of ω_+ was not observed up to 80 GHz and also between 107 and 124 GHz. This implies that there is a finite zero-field gap between ω_+ and ω_- and that the zero-field frequency of the ω_+ mode probably lies between 80 and 107 GHz. An estimate of this is made in Sec. V. There is also a finite jump at H_0 for the high-field branch of the ω_- mode.

B. AFMR Modes for H‖b

Figure 5 shows the frequency-field diagram for $\mathbf{H}\|b$ axis. Starting with the zero-field frequency, the resonance frequency increases with the magnetic field. At 72 GHz and about 5.3 kOe a discontinuity occurs. At this discontinuity a weak "resonance" of unusual shape was observed at various frequencies between 9 and 72 GHz. Above 5.3 kOe two resonances are again observed whose resonance frequencies increase as the magnetic field is increased. With the help of Figs. 4 and 5, the angular dependence in the bc' plane shown in Fig. 3 (where the weak "resonance" at the critical field is not

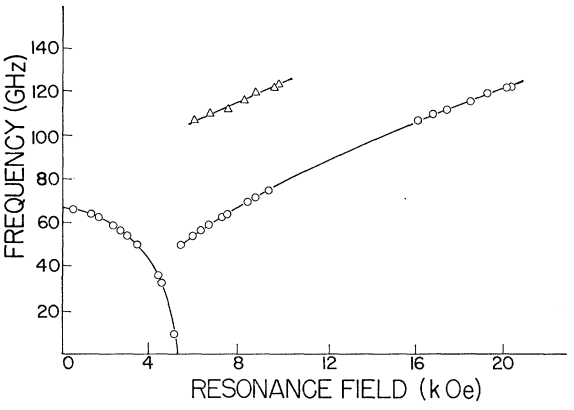

FIG. 4. AFMR frequency at 4.2°K plotted as a function of magnetic field along the c'' axis. The solid lines are smooth curves through the points.

[27] S. Foner and S. J. Williamson, J. Appl. Phys. **36**, 1154 (1965).

[28] The accuracy of the klystrons frequencies, as measured by the frequency meters, was better than ±0.2%. The accuracy of the magnetic field, measured by NMR probe, was found to be better than 1 part in 10^3 below 21 kOe. Above 21 kOe, the accuracy may be slightly worse. In most cases the sizes of the data points exaggerate the error in magnetic field and frequency.

[29] Because of the experimental difficulty of orienting the crystals in the bc'' plane, the angular dependence in this plane could not be studied (angle between c' and c'' being 8.5°). However, it is believed that the inferences drawn from the angular dependence in the bc' plane do not change.

shown) can now be understood. For example, no resonance is observed along the b axis below about 60 GHz. As H is rotated from along c' towards the b axis, the resonance line broadens. The effect is quite dramatic at 50 GHz where the resonance was observed in only about half the bc' plane as shown in Fig. 3. The angular dependence of the ω_+ mode in the bc' plane at two different frequencies is shown in Fig. 6. The resonance field is an extremum along the b and c' axes. The linewidth at 106.8 GHz varied from about 110 Oe in the b direction to about 170 Oe in the c' direction.

The usual shape of the weak "resonance" observed at the discontinuity is shown in Fig. 7. It is noted that χ'' will be a step function with a width of about 50 Oe. The resonance field for this resonance varied between 5.25 and 5.3 kOe at different frequencies with no definite pattern. The hysteresis of this resonance is no more than 10 Oe. Gyorgy[11] has also observed a discontinuous increase in the magnetization along b at about 5.3 kOe with negligible hysteresis. This is consistent with the AFMR observations.

C. AFMR Modes for H||a''

The frequency-field diagram for $\mathbf{H}\|a''$ is shown in Fig. 8. The resonance frequency decreases with the magnetic field but at a much slower rate compared to the c''-axis case. This difference between the a'' and c'' axes is clearer from the angular dependence in the ac plane shown earlier in Fig. 2. At 36 GHz and lower frequencies, the resonance field for a'' is higher than was available at these frequencies. Moreover, the AFMR line is broader along a'' than along c'' and the linewidth along a'' increases as the frequency decreases; the peak-to-peak linewidth at 64.9 GHz is 140 Oe, whereas at 50 GHz the linewidth is 375 Oe. By simple extrapolation, the spin-flop field (where $\omega=0$) for a'' is estimated to be in the neighborhood of 20 kOe.

At 33 and 36 GHz, another resonance (also shown in Fig. 8) with the minimum resonance field near the a axis was also observed. This resonance broadens out

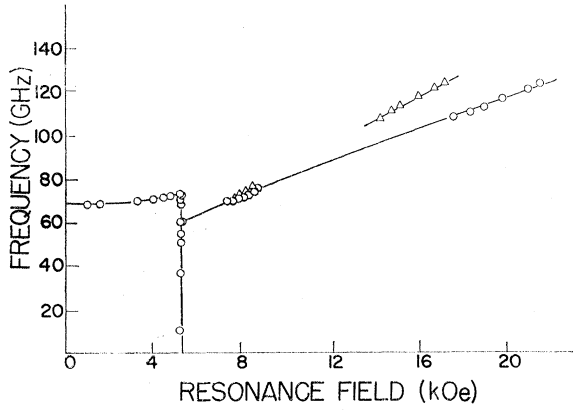

FIG. 5. AFMR frequency at 4.2°K plotted against magnetic field $\mathbf{H}$ for $\mathbf{H}\|b$ axis. The solid lines are smooth curves through the points.

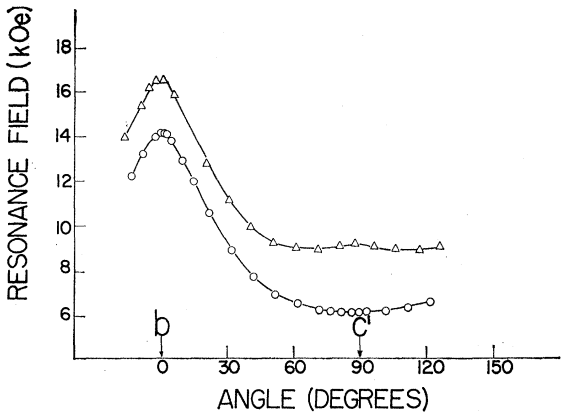

FIG. 6. Angular dependence of the resonance field for the ω_+ mode in the bc' plane at 4.2°K. △:120.0 GHz; ○:106.8 GHz. The solid lines are smooth curves through the points.

in an angular rotation of about $\pm 10°$ about the a axis. The ω_+ mode along a'' was not observed with the available magnetic field. The reason for this behavior becomes clear from Fig. 9, where the angular dependence of the resonance field of this mode in the ac plane is shown. The angular dependence varies almost as $1/\cos\theta$, where θ is measured from the position of the minimum resonance field which in this case is not along c''.

The angular dependence of the AFMR modes in the ab plane was studied only at 59.8 and 36.4 GHz since the observations were completely consistent with the data in the ac and bc' planes.

D. Temperature Dependence

The temperature dependence of the AFMR was studied only for the ω_- mode along c''. This temperature dependence of the resonance field between 1.4 and 15°K and 59.8 and 36.3 GHz is shown in Fig. 10. Note the "premature vanishing" of the low-field branch at 59.8 GHz. In Sec. V, these data are used to evaluate the temperature dependence of H_{11c}.

E. AFMR Linewidths

The temperature dependence of the AFMR linewidth along c'' at 59.8 GHz is shown in Fig. 11. As noted

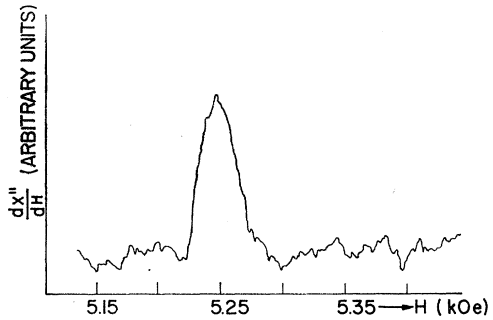

FIG. 7. A recorder trace of the "resonance" ($d\chi''/dH$ versus H) at the critical field along b at 4.2°K and 9.37 GHz.

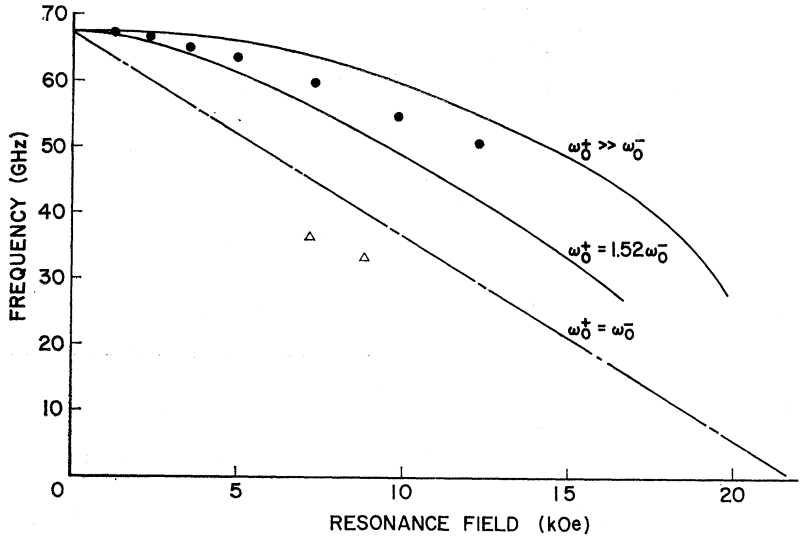

FIG. 8. ●: AFMR frequency at 4.2°K versus magnetic field along the a'' axis. △: Additional resonance (see text) with the minimum resonance field along the a axis. The data correspond to the minimum resonance field. The three curves are based on calculations (see Sec. V C).

earlier, the temperature dependence below 4.2°K is negligible and the residual temperature-independent linewidth is about 30 Oe.

The angular dependence of the AFMR linewidth for the high-field branch of ω_- mode in the ac plane is shown in Fig. 12. The data shown were taken at 59.8 GHz and at 4.2 and 1.4°K. For weak ferromagnets having isotropic g tensors, like $MnCo_3$ and α-Fe_2O_3, Turov has shown[30] that the angular dependence of the linewidth can be described by $\Delta H = \Delta H_{11}/\cos\theta$, where ΔH_{11} is the linewidth for H parallel to the position of minimum resonance field. For $Cu(HCOO)_2 \cdot 4H_2O$, in the WF state ($H > H_0$), one does observe sharp broadening of the line as a'' is approached. However, the minimum in the linewidth does not occur along c'', the position of minimum resonance field. This may result from g-tensor anisotropy since the principal axes of the g tensor do not coincide with a'' and c''.

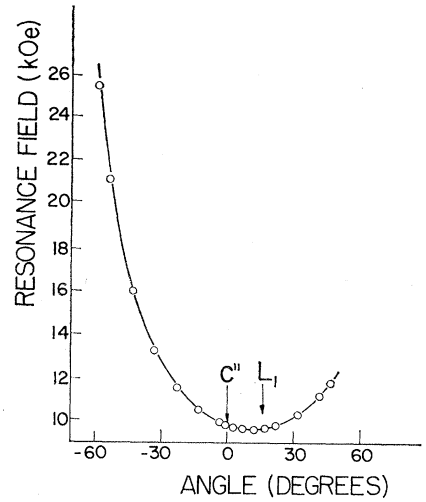

FIG. 9. Angular dependence of the resonance field for the high-field branch of the ω_+ mode at 4.2°K. ○: 123.8 GHz. The solid line is a smooth curve through the points.

[30] E. A. Turov, in *Physical Properties of Magnetically Ordered Crystals* (Academic Press Inc., New York, 1965), Chap. IX, p. 161.

V. COMPARISON OF EXPERIMENTAL RESULTS WITH THEORY AND DISCUSSION

A. H‖c'' Axis

Comparison of the experimental data shown in Fig. 4 is now made with the calculated resonance modes of Eqs. (15) and (16). For the low-field branch of the ω_- mode, a straight line is obtained by plotting $(\omega_-/\gamma)^2$ versus H^2_Y as Eq. (15b) demands. This fit yields $H_{DM'} = 8.6\times10^4$ Oe, $H_{11c}^2 = 5.2\times10^8$ Oe^2, and $H_0 = 5.28$ kOe. For the high-field branch of ω_-, $(\omega_-/\gamma)^2$ plotted versus H_Y yields a straight line as required by Eq. (16b). This gives $H_{DM'} = 8.5\times10^4$ Oe. For the ω_+ mode, $(\omega_+/\gamma)^2 - H_Y^2$ plotted versus H_Y [according to Eq. (16a)] yields a straight line with the slope $H_{DM'} = 8.2\times10^4$ Oe and the zero-field intercept $H_{11b}^2 - H_{11c}^2 = 6.8\times10^8$ Oe^2. This consistent value of $H_{DM'}$, obtained

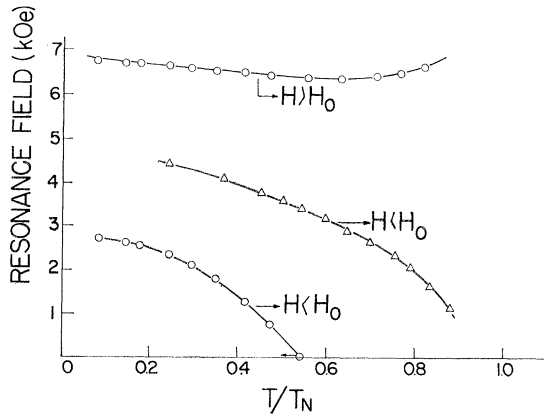

FIG. 10. Resonance field for the low- and high-field branches of the ω_- mode along c'' is plotted against reduced temperatures T/T_N, where $T_N = 17$°K. ○: 59.8 GHz; △: 36.3 GHz.

from the slopes of the three different branches of the AFMR modes, is one of the most convincing tests for the model used in the calculations of Sec. III.

Using $H_{DM'}=(8.4\pm0.2)\times10^4$ Oe, $H_{\|c}^2=5.2\times10^8$ Oe^2, $H_{\|b}^2-H_{\|c}^2=6.8\times10^8$ Oe^2, and Eqs. (15) and (16), we have plotted the AFMR frequency as a function of magnetic field in Fig. 13. The experimental points are also shown for comparison. There is good agreement between theory and experiment throughout except for the high-field branch of ω_- where a constant gap exists between the two. Empirically one may add an extra gap H_Δ^2 to Eq. (16b) giving

$$(\omega_-/\gamma)^2=H_Y H_{DM'}-H_{\|c}^2+H_\Delta^2, \quad H>H_0. \quad (35)$$

The experimental data then give $H_\Delta^2=2.75\times10^8$ Oe^2. This corresponds to a gap of 49 GHz at $H=H_0$. By taking into account the higher-order terms in the calculation, one in general obtains a gap at H_0. However, the magnitudes of these terms in the present case are very small and the predicted jump is only 0.2 GHz—too small to explain the observations. Therefore, there must be some other source for H_Δ^2. In $MnCo_3$, a weak ferromagnet of the easy-plane type, Borovik-Romanov *et al.*[31] observed an extra gap which decreased linearly with increasing temperatures. The temperature dependence of H_Δ^2 can be evaluated by using Eq. (32) and the temperature dependence of the resonance field (for $H>H_0$) shown in Fig. 10. Contrary to the case of $MnCo_3$ it is found that H_Δ^2 increases monotonically with temperature. Therefore, at present the physical origin of H_Δ^2 is not known. The low-field branch of the ω_+ mode has not been observed, but using the above numbers the predicted zero-field value for this mode is 102.5 GHz.

From the fit of the paramagnetic susceptibility to the high-temperature series expansion, J_{jk} (the Heisenberg exchange between a pair of nearest-neighbor ions) was found to be 71.5°K.[6] From Eq. (4) $H_{ex}=J\langle S\rangle/2\mu_B$, where $J=zJ_{jk}$. z is the number of nearest neighbors coupled by strong exchange and is considered to be 4 in this case. Using $\langle S\rangle=\frac{1}{2}$ [32] one finds $H_{ex}=1.06\times10^6$ Oe. Although $g_{22}=2.34$ has been determined from g-value measurements in the paramagnetic region,[7] it is not possible to determine the off-diagonal components without knowledge of the asymmetric contribution to the g tensor. Therefore, one cannot determine the other exchange constants H_{DM}, H_K, h_{DM}, H_A, and $H_{K'}$. We shall return to this question later.

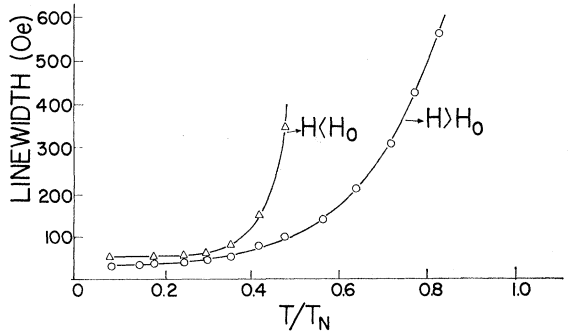

FIG. 11. Temperature dependence of the AFMR linewidth at 59.8 GHz for the ω_- mode along c''.

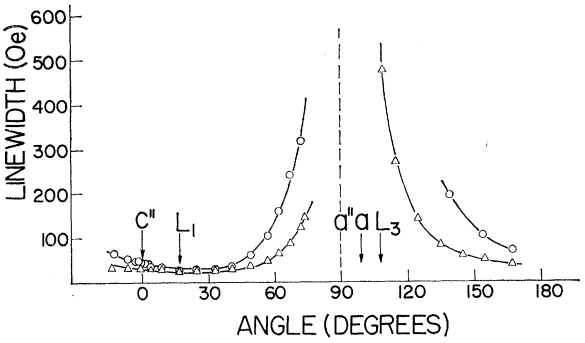

FIG. 12. Angular dependence of the AFMR linewidth at 59.75 GHz for the high-field branch of the ω_- mode. ○: 4.2°K; △: 1.4°K. The solid lines are smooth curves through the points.

Using the values of H_{ex}, $H_{DM'}$, $H_{\|c}$, and g_{22} and Eqs. (9) and (10) one can calculate the magnetization and the susceptibility ratio along the c'' axis. The calculated value for the field-induced weak moment is found to be 2.02 (cgs emu)/cm^3. From Eq. (10) one obtains $\chi_{\perp,Y}^{AF}/\chi_{\perp,Y}^{WF}=1+(H_{DM'}/H_{\|c})^2=15.2$. Magnetization data along c'' are not available; however, the measurements of KH[4] along L_1 (L_1 is 17° away from c'' in the ac'' plane) may be used to make a crude check on the above values. The KH data give M_0^{WF}(along L_1) ≈1.25 (cgs emu)/cm^3 and $\chi_{L_1}^{AF}/\chi_{L_1}^{WF}\approx10$.

B. H$\|b$ Axis

It has not been possible to obtain a good quantitative fit of the AFMR modes for this case to Eqs. (32a) and (32b). However, one can explain some of the qualitative features of the mode spectrum. It is useful to take the difference of (32b) and (32a) because the term containing the effective canting field $H_{DM}*$ cancels out. The result is

$$(\omega_-/\gamma)^2-(\omega_+/\gamma)^2=H_{\|b}^2(1-\sin^2\theta)-H_{\|b}^2-H_X^2. \quad (36)$$

This expression yields information on the critical

[31] A. S. Borovik-Romanov, N. M. Kreines, and L. A. Prozorova, Zh. Eksperim. i Teor. Fiz. **45**, 64 (1963) [English transl.: Soviet Phys.—JETP **18**, 46 (1964)].

[32] Our assumption of $\langle S\rangle=\frac{1}{2}$ neglects the effect of the zero-point spin deviations. For a two-dimensional spin-$\frac{1}{2}$ Heisenberg AF, the spin-wave theory gives $\langle S\rangle=0.31$ [see P. W. Anderson, Phys. Rev. **86**, 694 (1952)]. If such large deviations are present, the stability of the Néel state is questionable [see F. Keffer, in *Encyclopedia of Physics* (Springer-Verlag, Berlin, 1966), Vol. 18, p. 139]. However, the effect of the anisotropy, which is quite significant in the present case, is to decrease the spin deviations and to stabilize the Néel state. Since no other independent check on the values of the exchange parameters is available, we cannot get an estimate on the spin deviations from the present experiments. A deviation from $\langle S\rangle=\frac{1}{2}$ will effect the values of the derived constants such as H_{DM}, H_K, and $H_{K'}$. However, the ratio $H_K/H_{K'}$ remains unchanged.

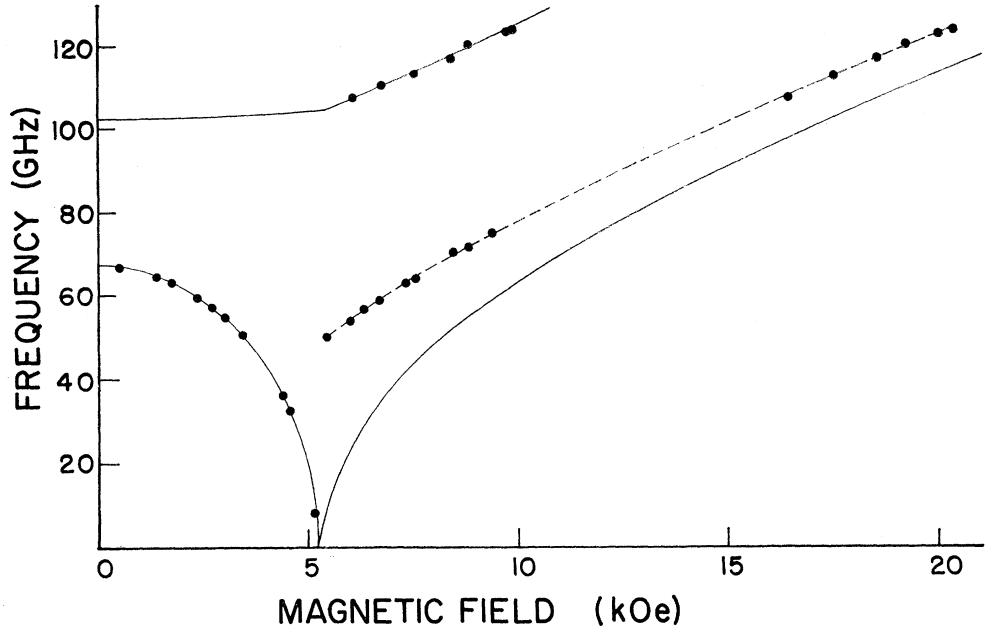

FIG. 13. Comparison between theory and experiment for $\mathbf{H}\|c''$ axis. The solid lines are thoeretical curves using $H_{DM'}=8.4\times10^4$ Oe, $H_{11c}^2=5.2\times10^8$ Oe^2, and $H_{11b}^2-H_{11c}^2=6.8\times10^8$ Oe^2. The solid circles are experimental points.

angles θ_{c1} and θ_{c2}. Figure 5 indicates that the two modes are nearly degenerate just above the instability field H_c leading to $\cos^2\theta_{c2}\approx0.46$ using the values for H_{11c}, H_{11b}, H_c, and $g_{11}=2.11$. Equation (36) also indicates that the frequency difference between the two modes must decrease as $\mathbf{H}$ increases from zero. Furthermore, (32a) indicates that for ω_+ to increase (not considering for the present the $H_XH_{DM}^*$ term) $\sin^2\theta$ must remain very small ($H_{11b}^2\sin^2\theta<H_X^2$). At H_c- we set

$$(\omega_-/\gamma)^2-(\omega_+/\gamma)^2=H_{11b}^2-H_{11c}^2-H_{\Delta'}^2$$

and obtain

$$\sin^2\theta_{c1}=[H_{\Delta'}^2-(\tfrac{1}{2}g_{11})^2H_c^2]/H_{11b}^2.$$

$H_{\Delta'}>(\frac{1}{2}g_{11})H_c$ is required, but it cannot be very large since $\sin\theta$ must change slowly with field. Hence $\sin^2\theta_{c1}\ll1$, probably less than 0.01. As the field is increased above H_c, $(\omega_--\omega_+)$ slowly increases as seen in Fig. 5. (The angular dependence of the modes in the bc' plane in the high-field region indicates that ω_- remains the higher-frequency mode for $H>H_c$.) This implies that $\sin^2\theta$ decreases from $\sin^2\theta_{c2}$ for H increasing above H_c. The value of $\sin\theta$ for $H>H_c$ can be calculated, in principle, from Eq. (22).

Employing Eqs. (25a) and (25b) and the values of θ_{c1} and θ_{c2} obtained from (36) and Fig. 5, one obtains $\lambda\approx0.70$ and $H_{DM''}/|h_{DM'}|\approx0.02$ for $\sin\theta_{c1}=0.05$. λ is quite insensitive to the value of $\sin\theta_{c1}$ chosen (it does depend on $\cos\theta_{c2}$), however, the ratio $H_{DM''}/|h_{DM'}|$ increases almost proportionately to $\sin\theta_{c1}$. From the definition of λ one then obtains $|h_{DM'}|\approx8.6\times10^4$ Oe and $H_{DM''}\sim10^3$ to 3×10^3 Oe depending on the value of $\sin\theta_{c1}$ chosen. Both these values will be altered by changes in θ_{c2}. This analysis suggests that $|h_{DM'}|$ is of the same order of magnitude as $H_{DM'}$ but that $H_{DM''}$ is very much smaller than either of these quantities.

The problem with the above analysis is that it predicts a rather large H_{DM}^* which is always negative for the allowed range of θ. It introduces a very large negative contribution to ω_+ and ω_- at large fields and also contributes a zero-field component to the magnetization [see Eq. (27)]. Even if one uses an $H_{DM\,eff}^*=H_{DM}^*(\theta)-H_{DM}^*(0)$, that requires the H_{DM}^* employed in (32a) and (32b) to be zero at H and $\theta=0$ the agreement at large fields is poor. The calculated modes show a tendency to flatten out at high fields, whereas Fig. 5 indicates both ω_+ and ω_- appear to be increasing linearly with field at high fields. It would seem that a positive H_{DM}^* which increases with field is required to explain the b-axis results; however, this is inconsistent with the negative $h_{DM'}$ required to explain the instability.

The magnetization data for $H\ll H_c$ are also not in satisfactory agreement with the above results. If one takes the ratio $\chi_{\perp,X}^{AF}$ to $\chi_{\perp,Y}^{AF}$ employing Eqs. (29) and (9a), one obtains

$$\frac{\chi_{\perp,X}^{AF}}{\chi_{\perp,Y}^{AF}}=\left(\frac{g_{11}}{g_{22}}\right)^2\frac{[1+(H_{DM''}/H_{11b})^2]}{[1+(H_{DM'}/H_{11c})^2]},\quad H\ll H_c. \tag{37}$$

Since $H_{DM''}$ appears to be much less than H_{11b}, the result is about $(2.11/2.34)^2/15.2\sim0.053$. The results of KH[4] for $\mathbf{H}\|b$ and $\mathbf{H}\|L_1$ (17° from c'') indicate a ratio closer to $\frac{1}{2}$. For $H>H_c$ the magnetization data of KH for L_1 and the b axis (L_2) are very similar. This would only be the case [see Eq. (27)] if H_{DM}^* were approximately $H_{DM'}$ for large fields. This is strongly incon-

sistent with the above discussion. Thus neither the magnetization data nor the AFMR modes for $\mathbf{H}\|b$ can be satisfactorily explained. Nevertheless, the calculations of the AFMR modes do indicate the possibility of explaining the observed instability with a Hamiltonian just including bilinear exchange terms.

C. $\mathbf{H}\|a''$

The data for this case are shown in Fig. 8. The data are rather incomplete; however, the lower mode ω_- is shown out to about 12 kOe, the frequency having dropped from 67.3 GHz to about 50 GHz. The two data points (Δ) at 36 and 33 GHz between 7 and 9 kOe are not understood at present.

Theoretical expressions are also shown in Fig. 8 based on Eq. (34) (the procedure was outlined in the Appendix). For $\omega_{+0}=\omega_{-0}$ ($H_{\|b}=H_{\|c}$), Eq. (34) reduces to the expression given by Foner and Williamson, and this falls well below the experimental data. The extreme limit $\omega_{+0}\gg\omega_{-0}$ ($H_{\|b}\gg H_{\|c}$) is also shown and lies above the experimental values. The intermediate curve is for the estimated experimental value $H_{\|b}/H_{\|c}=1.52$. It is only in fair agreement with the experimental results. A larger ratio $H_{\|b}/H_{\|c}$ would make the agreement better; however, this cannot be considered significant since all effects of canting have been neglected in finding the equilibrium position. Note that the calculated spin-flop field $H_{sf}=(2/g_{33})H_{\|c}=21.8$ kOe. This was not determined experimentally. Substantially more data are required before a complete analysis of the a''-axis results is feasible.

D. Estimate of Other Exchange Parameters

The problem of obtaining the parameters H_K, $H_{K'}$, H_{DM}, and h_{DM} is a complex problem and requires detailed knowledge of the components of the asymmetric g tensor. Since these components are not determined from conventional EPR experiments we can at best make estimates neglecting the antisymmetric contributions. The symmetric g-tensor assumption gives $g_{12}=g_{21}=0.08$ [20] and yields $H_{DM}\sim 12$ kOe, which would also require $H_{DM''}=-H_{DM}+2H_{ex}g_{12}/g_{11}=68$ kOe, which is a much larger value than indicated in Sec. V B.

TABLE I. Values of exchange constants and AFMR mode parameters at 4.2°K.

H_{ex}	$(1.06\pm0.05)\times10^6$ Oe[a]	
$H_{\|c}$	2.28×10^4 Oe	
$H_{\|b}$	3.46×10^4 Oe	
$H_{DM'}$	$(8.4\pm0.2)\times10^4$ Oe	
	$g_{21}=0.08$	$g_{21}=0.06$
H_{DM}	12×10^3 Oe[b]	30×10^3 Oe[b]
H_{K^-}	3.1×10^2 Oe[b]	6.7×10^2 Oe[b]
$H_{K'}$	1.6×10^2 Oe[b,c]	1.6×10^2 Oe[b,c]
H_K	4.7×10^2 Oe[b,c]	8.3×10^2 Oe[b,c]

[a] Based on the J_{jk} value of Ref. 6.
[b] Based on symmetric g tensor.
[c] It has been assumed that $h_{DM}\ll H_{DM}$.

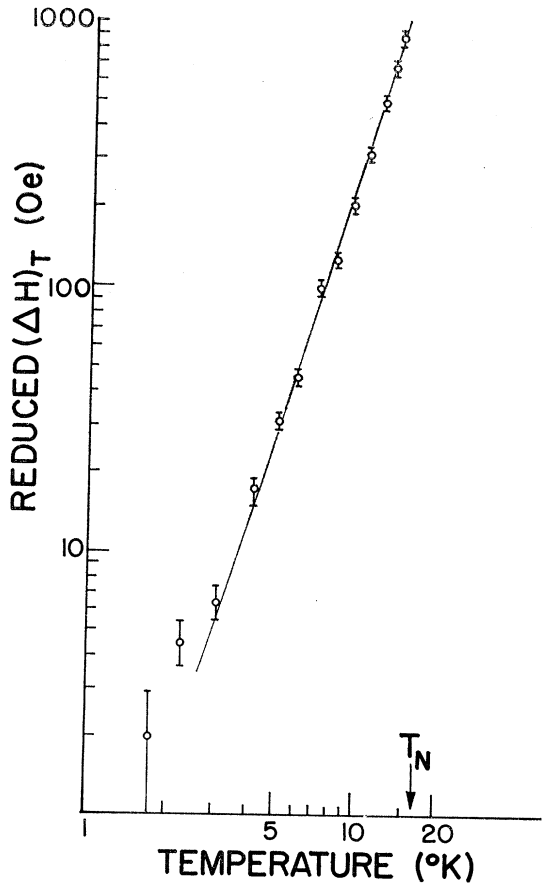

FIG. 14. Reduced AFMR linewidth $(\Delta H)_T\propto T^n$ is plotted against temperature on a log-log plot. The solid line is the best fit through the data points giving $n=3.3\pm0.2$.

Employing $H_{\|c}^2$, H_{DM}, and H_{ex}, one finds $H_{K^-}=313$ Oe. $H_{K'}$, and hence H_K, cannot be obtained from $(H_{\|b}^2-H_{\|c}^2)$ unless h_{DM} is known. The copper formate geometry[20] and Moriya's rules for the direction of the $\mathfrak{D}_{jk}$ [33] suggest either $h_{DM}\ll H_{DM}$ or that $h_{DM}/H_{DM}\sim4$–5. This latter choice would require a rather large negative $H_{K'}$, which is inconsistent with $Z(a'')$ as the easy axis. If $h_{DM}\ll H_{DM}$ then one finds $H_{K'}=160$ Oe and $H_K=473$ Oe. As an illustration of the effect of small changes in the g tensor on these exchange parameters, a calculation of these same quantities is shown in Table I, along with the above values, for $g_{21}=g_{12}=0.06$ and $h_{DM}\ll H_{DM}$.

The value of $H_{DM}\sim12$ kOe obtained above is in good agreement with the value of $|\mathfrak{D}|$ inferred from the exchange-narrowed EPR linewidth[8] measured at high temperatures ($70<T<273$°K). It is rather risky, however, to compare the H_{DM} measured by AFMR at 4.2°K with that inferred from EPR linewidth measured at much higher temperatures. Moriya[33] has estimated the magnitude of H_{DM} to be about $(\Delta g/g)H_{ex}$ which would imply (for $\Delta g/g\sim0.13$) an H_{DM} an order of

[33] T. Moriya, Phys. Rev. Letters 4, 228 (1960); Phys. Rev. 120, 91 (1960).

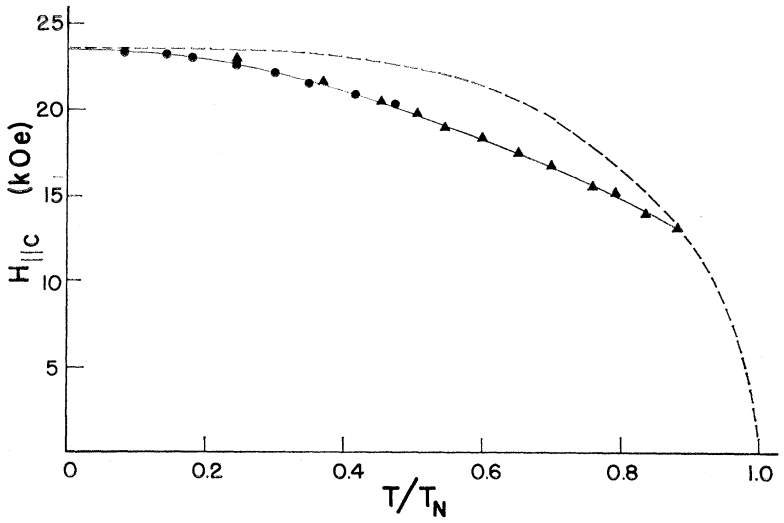

FIG. 15. Derived values of $H_{\|c}$ versus T/T_N. The dashed curve is the normalized Brillouin function for $S=\frac{1}{2}$. The solid curve is a smooth curve through the points. ●: 59.75 GHz; ▲: 36.3 GHz.

magnitude larger than 12 kOe. As Table I indicates for $g_{21}=0.06$, a somewhat larger value of H_{DM} is certainly possible; however, a value an order of magnitude larger seems unreasonable and would require a negative value for g_{21}.

The data for $\mathbf{H}\|b$ suggest a large negative $h_{DM'}$. However, if $|h_{DM}|\ll H_{DM}$ this can only be achieved by a large negative value of $g_{13}(g_{13}\sim -0.16)$. It is not known whether this value is realistic. No definite conclusions can be reached concerning the magnitude of h_{DM}. We note, however, that for both the $\mathbf{H}\|c''$ and $\mathbf{H}\|b$ cases the effective canting fields $H_{DM'}$, $H_{DM''}$, and $h_{DM'}$ have large contributions due to the antisymmetric Zeeman interaction. For $H_{DM'}$, which is much better known than $H_{DM''}$ and $h_{DM'}$, the analysis indicates that the contribution of the antisymmetric Zeeman term is the dominant canting term.

E. Temperature Dependence of $H_{\|c}$

From the temperature dependence of the resonance field for the ω_- mode (Fig. 10) and Eq. (15b), we have determined the temperature dependence of $H_{\|c}$. (Note that H_{ex}, H_K, H_{DM}, etc., are proportional to $\langle S\rangle$, which is temperature dependent. The ratio $(H_{DM'}{}^2/H_{\|c}{}^2)$ is temperature independent.) This analysis yields the temperature dependence shown in Fig. 14. The value of $H_{\|c}$ extrapolated to zero temperature is 23.5 kOe compared with 22.5 kOe at 4.2°K. Since both $H_{\|c}$ and the magnetization are proportional to $\langle S\rangle$, the temperature dependence of the magnetization should be the same as that of $H_{\|c}$. On the molecular field approximation, the magnetization should vary as the normalized Brillouin function for $S=\frac{1}{2}$. The deviation from this behavior, as shown in Fig. 14, may not be surprising since the molecular field approximation was found to be a poor approximation even in the paramagnetic region. This deviation has been attributed to a two-dimensional Heisenberg-like behavior.[6] Recently, Birgeneau *et al.*[34] found that in Rb_2MnF_4, a two-dimensional near-Heisenberg AF, the magnetization also deviates from the molecular field approximation. Instead, their results indicate that the magnetization follows a $(T_N-T)^{0.18}$ law from $T_N=38.4$°K to $T_N=4.3$°K. A similar analysis has been done for the present case. The data fit reasonably well the relation $(T_N-T)^{0.30}$ from 1.4 to 15°K.

F. Temperature Dependence of AFMR Linewidth

The experimental linewidth shown in Fig. 11 has a temperature-dependent and a temperature-independent contribution. The temperature-independent residual linewidth of about 30 Oe presumably arises from the crystal defects. Such residual AFMR linewidths have been observed in all materials; e.g., the residual linewidth is 300 Oe in MnF_2 [35] and 20 Oe in $CuF_2\cdot 2H_2O$.[36]

The temperature dependence of the AFMR linewidth for a uniaxial antiferromagnet with $H_{DM'}=0$ has been considered by various authors but the results are in disagreement with one another. In the limit of $kT\gg\hbar\omega_0$ $[\omega_0/\gamma=(2H_{ex}H_K)^{1/2}]$ the temperature dependence of the AFMR linewidth is shown proportional to T by Urushadze,[37] T^2 by Kawasaki,[38] and Tani,[39] and T^3 by Harris.[40] For the present case with $H_{DM'}\neq 0$, it is doubtful whether any of these theories is applicable.

The theoretical expression for the linewidth is usually given at constant magnetic field, whereas the experimental linewidths measured here were determined at constant frequency. Therefore, a conversion factor $(1/\gamma)(\partial\omega/\partial H)$, whose values can be determined from

[34] R. J. Birgeneau, H. J. Guggenheim, and G. Shirane, Bull. Am. Phys. Soc. **14**, 738 (1969).
[35] F. M. Johnson and A. H. Nethercot, Phys. Rev. **114**, 705 (1959).
[36] K. Nagata and M. Date, J. Phys. Soc. Japan **21**, 2420 (1966).
[37] G. I. Urushadze, Zh. Eksperim. i Teor. Fiz. **39**, 680 (1960) [English transl.: Soviet Phys.—JETP **12**, 476 (1961)].
[38] T. Kawasaki, Progr. Theoret. Phys. (Kyoto) **34**, 357 (1965).
[39] K. Tani, Progr. Theoret. Phys. (Kyoto) **31**, 335 (1964).
[40] A. B. Harris, J. Appl. Phys. **37**, 1128 (1966).

the resonance conditions (15) and (16), is used. The reduced temperature-dependent contribution to the linewidth $(\Delta H)_T$ is plotted versus temperature on a log-log plot in Fig. 15. The best fit with the data, shown by the solid line, yields the law $(\Delta H)_T \propto T^{3.3\pm0.2}$. The deviation from this law below about 4.2°K may simply be related to H_{11c}, which is approximately 3.2°K.

ACKNOWLEDGMENTS

The authors are particularly grateful to Professor E. Jacobsen for the loan of much of the 2.5- and 5-mm microwave components, in addition to two mm-wavelength klystrons, which made this work possible. They are also thankful for two other klystrons kindly lent by Professor D. Douglass and Professor S. Shapiro. Beneficial discussions with Dr. I. Jacobs, Dr. M. E. Lines, Dr. F. B. Hagedorn, Dr. E. M. Gyorgy, and Dr. R. J. Birgeneau are gratefully acknowledged.

APPENDIX: CALCULATION OF AFMR MODES FOR H$\|a''$

This calculation is similar to that for a uniaxial AF[41] but includes two anisotropy fields H_K and $H_{K'}$ the latter representing the hard-plane anisotropy. For simplification we set the unknown cant angle α (see Fig. 1) equal to zero ($H_A = h_{DM} = 0$) so that we assume the two sublattices exactly antiparallel along Z (a''). In determining the equilibrium position we neglect all canting terms such as the DM interaction or the antisymmetric Zeeman interaction. The equilibrium positions will then be antiparallel along Z for the magnetic field below the spin-flop critical field. The transformation equations from X, Y, Z to the sublattice equilibrium positions are $(i=1,2)$

$$\begin{aligned} X_i &= (-1)^{i+1}X_i', \\ Y_i &= Y_i', \\ Z_i &= (-1)^{i+1}Z_i'. \end{aligned} \tag{A1}$$

[41] For a review of the AFMR modes for uniaxial AF, see the review article by S. Foner, in *Magnetism*, edited by G. Rado and H. Suhl (Academic Press Inc., New York, 1963), Vol. I., pp. 390–407.

The Hamiltonian analogous to Eq. (12) will be

$$\begin{aligned} \mathcal{H} = H_{ex}(&-X_1'X_2' + Y_1'Y_2' - Z_1'Z_2') \\ &- H_K Z_1'Z_2' - H_{K'}(X_1'X_2' + Y_1'Y_2') \\ &- H_{DM}(X_1'Y_2' + Y_1'X_2') - \tfrac{1}{2}g_{31}H(X_1' + X_2') \\ &- \tfrac{1}{2}g_{32}H(Y_1' + Y_2') - \tfrac{1}{2}g_{33}H(Z_1' - Z_2'). \end{aligned} \tag{A2}$$

Particular note of the diagonal Zeeman term should be taken. It is antisymmetrical in Z_1' and Z_2' rather than symmetrical as in Eq. (12). Equation (A2) then leads to the following set of linearized equations of motion:

$$\begin{aligned} -i\omega/\gamma X_1' &= B_Z Y_2' - C_Z Y_1' + F_Z X_2' - c_Z Y_1', \\ -i\omega/\gamma X_2' &= B_Z Y_1' - C_Z Y_2' + F_Z X_1' + c_Z Y_2', \\ -i\omega/\gamma Y_1' &= -A_Z X_2' + C_Z X_1' - F_Z Y_2' + c_Z X_1', \\ -i\omega/\gamma Y_2' &= -A_Z X_1' + C_Z X_2' - F_Z Y_1' - c_Z X_2', \end{aligned} \tag{A3}$$

where

$$\begin{aligned} A_Z &= -H_{ex} - H_{K'}, \\ B_Z &= H_{ex} - H_{K'}, \\ C_Z &= -H_{ex} - H_K, \\ F_Z &= -H_{DM}, \end{aligned}$$

and

$$c_Z = (\tfrac{1}{2}g_{33})H = H_Z.$$

Note that the canting term H_{DM} is included when determining the mode frequencies.

Taking the natural mode linear combinations, namely, $X_1'+X_2'$, $Y_1'+Y_2'$ and $X_1'-X_2'$, $Y_1'-Y_2'$, the solution for the AFMR modes is a determinant of the form

$$\begin{vmatrix} i\omega/\gamma + F_Z & (B_Z - C_Z) & 0 & -c_Z \\ -(A_Z - C_Z) & i\omega/\gamma - F_Z & c_Z & 0 \\ 0 & -c_Z & i\omega/\gamma - F_Z & -(B_Z + C_Z) \\ c_Z & 0 & (A_Z + C_Z) & i\omega/\gamma + F_Z \end{vmatrix} = 0. \tag{A4}$$

Multiplication of (A4) yields the equation

$$\begin{aligned} (\omega/\gamma)^4 - (\omega/\gamma)^2[H_{11b}^2 + H_{11c}^2 + 2c_Z^2] \\ + (H_{11b}^2 - c_Z^2)(H_{11c}^2 - c_Z^2) = 0, \end{aligned} \tag{A5}$$

where γH_{11b} and γH_{11c} are, respectively, the zero-field resonance mode frequencies $\omega_+(0)$ and $\omega_-(0)$ where H_{11b} and H_{11c} are given by

$$\begin{aligned} H_{11b} &= (A_Z + C_Z)(B_Z + C_Z) - F_Z^2, \\ H_{11c} &= (A_Z - C_Z)(B_Z - C_Z) - F_Z^2. \end{aligned} \tag{A6}$$

Solution of Eq. (A5) leads directly to the modes ω_+ and ω_- given in Eq. (34).